*International Journal of Marine Engineering Innovation and Research, Vol. 11(1), Mar. 2026. 9-22*
*(pISSN: 2541-5972, eISSN: 2548-1479)*



# Engine Combustion Performance and Emission of a Dual-Fuel NH3-B100 in Yanmar TF-85

Muayyad Z.A[1*], Aguk Zuhdi M. Fathallah[2]

(Received: 19 Januari 2026 / Revised: 20 January 2026 / Accepted: 4 Februari 2026 / Available Online: 15 March 2026)

***Abstract-***This study investigates the combustion characteristics, engine performance, and emission behavior of an ammonia–biodiesel ($NH_3$–B100) dual-fuel compression-ignition engine based on a Yanmar TF-85 diesel platform using a combined experimental and numerical approach. Three-dimensional (3D) in-cylinder combustion simulations were performed using ANSYS Forte, while overall engine performance was evaluated through a one-way 3D-1D coupling framework integrated with MATLAB. Baseline single-fuel B100 operation was first validated against experimental measurements, yielding prediction errors below [6%] for engine power, confirming the reliability of the simulation model. After validation, ammonia was introduced through intake manifold injection to establish dual-fuel operation. The results indicate that ammonia substitution delays combustion phasing and reduces the peak heat release rate by approximately [22%], leading to decreases in indicated mean effective pressure and brake power of [30%] and an increase in specific fuel consumption of [30%]. In terms of emissions, carbon-related species were reduced, with $CO_2$ and CO decreasing by up to [60%] and [50%], respectively, whereas $NO_x$ emissions increased by [20%], and measurable $NH_3$ slip was observed under high ammonia energy fractions. Overall, the proposed 3D–1D modeling framework provides an accurate and computationally efficient tool for evaluating ammonia–biodiesel dual-fuel strategies and supports the development of low-carbon marine diesel engines.

*Keywords*--Dual-fuel combustion, Ammonia-biodiesel, CFD combustion simulation, Marine diesel engine, Emission characteristics

**Corresponding Author: okeybos78@gmail.com@ust.edu.ng*

## I. INTRODUCTION

The fossil fuel–based energy sector is facing increasing challenges due to climate change concerns and the need to reduce greenhouse gas (GHG) emissions. These pressures have accelerated the development of alternative, low-carbon, and carbon-free fuels for internal combustion engines (ICEs). In the maritime sector, shipping is recognized as a significant contributor to global emissions, prompting regulatory actions to promote cleaner propulsion technologies. According to the International Maritime Organization (IMO) 2023 GHG Strategy, key objectives include improving ship energy efficiency, reducing carbon intensity by at least 40% by 2030 relative to the 2008 baseline, and accelerating the adoption of zero- or near-zero-emission fuels [1-3].

In line with these decarbonization targets, increasing attention has been directed toward alternative chemical fuels that can be utilized within existing engine infrastructure [4,5]. Among the potential candidates, ammonia ($NH_3$) has emerged as a promising carbon-free energy carrier due to its absence of carbon in the molecular structure, relatively high hydrogen density, and established production and transportation systems. These characteristics make ammonia attractive for large-scale marine applications [6,7].

Despite these advantages, the direct use of ammonia in compression-ignition engines remains challenging due to its poor flammability, high autoignition temperature, and slow laminar flame speed, which often result in delayed ignition and unstable combustion [8,9]. To address these limitations, dual-fuel strategies have been widely investigated, where ammonia is combined with a more reactive pilot fuel to ensure reliable ignition [10-12]. Biodiesel (B100) is considered a suitable pilot fuel because of its higher cetane number, inherent oxygen content, and lower particulate emissions compared to conventional diesel, making it compatible with cleaner marine engine operation [13].

Previous studies have reported that ammonia–biodiesel dual-fuel combustion can substantially reduce carbon-related emissions. However, such an operation is frequently accompanied by reduced thermal efficiency, increased $NO_x$ formation, and ammonia slip due to incomplete oxidation [14,15]. Although these issues have been investigated individually, most existing works focus either on detailed combustion simulations or on overall engine performance analysis, while integrated approaches that simultaneously evaluate in-cylinder combustion processes, emissions formation, and brake-level engine performance remain limited.[16].

Therefore, this study proposes a coupled numerical framework integrating three-dimensional combustion simulations in ANSYS Forte with one-dimensional engine performance modeling in MATLAB to analyze the combustion characteristics, performances, and emission behavior of an ammonia-B100 dual fuel compression ignition engine based on a Yanmar TF-85 platform. The objective is to provide a comprehensive assessment of dual fuel combustion strategies and to evaluate their potential as low carbon solutions for future marine propulsion systems [17-19].

Muayyad Zainal Abidin, Institut Teknologi Sepuluh Nopember, Surabaya, Indonesia. Email: okeybos78@gmail.com@ust.edu.ng
Aguk Zuhdi M Fathallah, Institut Teknologi Sepuluh Nopember, Surabaya, Indonesia. Email: fathalaz@its.ac.id

## II. METHOD

### 2.1 Research Framework

This study employs a combined experimental and numerical methodology to investigate the combustion behavior, engine performance, and emission characteristics of a dual-fuel ammonia-biodiesel ($NH_3$-B100) diesel engine. The research framework consists of three sequential stages:

(i) baseline experimental testing of the original engine operating on single-fuel B100,
(ii) three-dimensional (3D) combustion simulation and model validation using ANSYS Forte, and
(iii) extension of the validated numerical framework to dual-fuel $NH_3$-B100 operation using a one-way, offline 3D–1D modeling approach.

This stepwise approach ensures that the numerical predictions are grounded in experimental data before being applied to dual-fuel combustion analysis (see Figure 1).

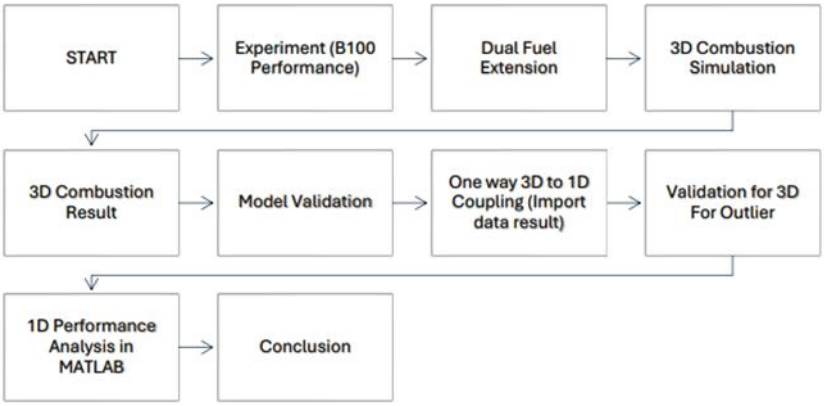


**Figure 1.** Method Flowchart

### 2.2 Engine Specifications and Baseline Experimental Setup

The engine investigated in this study is a Yanmar TF-85 single-cylinder, four-stroke, direct-injection diesel engine. The main engine specifications, including bore, stroke, compression ratio, rated power, and operating speed, are obtained from manufacturer data and are summarized in Table 1.

TABLE 1.
SPECIFICATION OF YANMAR TF-85

| | |
|---|---|
| Bore × Stroke | 85 mm × 87 mm |
| Volume Displacement | 493 $cm^3$ |
| Compression Ratio | 18:1 |
| Cylinder | 1 |
| Power Maximum | 6,2 kW / 2200 RPM |
| Diesel Injection Pressure / Timing | 19,6 MPa / -18 CA BTDC |

Baseline experiments were conducted using B100 as the sole fuel to establish reference engine performance and emission characteristics. Measured parameters include brake power, brake thermal efficiency, specific fuel consumption, and exhaust emissions. Due to limitations in combustion diagnostic instrumentation, in-cylinder combustion measurements were not performed experimentally; therefore, combustion-related analyses were primarily evaluated through validated numerical simulations.

### 2.3 Three-Dimensional Combustion Simulation

Three-dimensional combustion simulations were carried out using ANSYS Forte to analyze in-cylinder flow, spray dynamics, ignition, and combustion processes. The computational domain represents the full cylinder geometry and incorporates piston motion and valve events. Dynamic meshing techniques were employed to capture the transient nature of the engine cycle [19].

Fuel injection of B100 was modeled using a Lagrangian spray framework, incorporating sub-models for atomization, evaporation, and spray–turbulence interaction. Turbulence was modeled using the Reynolds-Averaged Navier–Stokes (RANS) approach, while combustion chemistry was represented using a reduced reaction mechanism suitable for biodiesel combustion. These modeling choices were adopted based on established practices reported in previous engine combustion studies [19,20,21].

Boundary and initial conditions were defined according to experimental operating conditions to ensure consistency between simulation and testing.

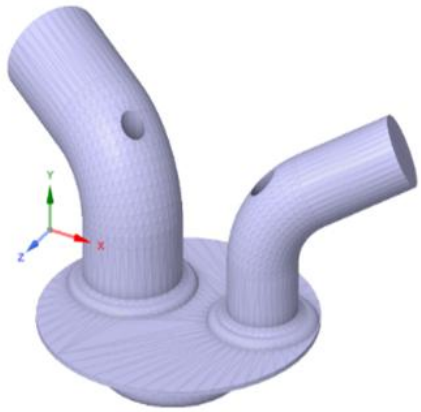

**Figure 2.** 3D Simulation Model

2.4 Model Validation

Model validation was performed by comparing numerical predictions with experimental results obtained from baseline single-fuel B100 operation. Validation focused on key performance indicators, including brake power, brake thermal efficiency, and specific fuel consumption trends [21].

The agreement between experimental and numerical results was quantified using relative error analysis. The observed level of agreement was considered acceptable for the purposes of this study, allowing the numerical framework to be used for further investigation of dual-fuel combustion behavior.

2.5 Dual-Fuel $NH_3$-B100 Combustion Modeling

After validation of the baseline model, the numerical framework was extended to simulate dual-fuel $NH_3$-B100 operation. In this configuration, ammonia was introduced through an intake manifold injection system, while B100 was retained as the pilot fuel injected directly into the cylinder. This strategy enables reliable ignition initiated by B100 while allowing ammonia to contribute to the total energy input.

Various ammonia energy fractions were investigated to evaluate their influence on combustion characteristics, engine performance, and emission behavior. The original engine geometry and operating conditions were maintained without major modifications to ensure direct comparability with baseline operation.

2.6 One-Way 3D-1D Modeling Framework

To evaluate overall engine performance, a one-way, offline 3D-1D modeling framework was implemented. Combustion-related outputs from the 3D ANSYS Forte simulations, such as in-cylinder pressure traces and heat release characteristics, were extracted and transferred to a MATLAB-based one-dimensional performance model.

This one-way data transfer approach enables performance evaluation without real-time co-simulation between solvers, reducing computational cost while preserving essential combustion information. The 1D model was subsequently used to calculate performance indicators, including brake thermal efficiency and engine output.

2.7 Data Analysis and Emission Evaluation

Combustion behavior was analyzed based on simulated in-cylinder pressure, heat release rate, ignition delay, and combustion phasing. Engine performance parameters were derived from the 1D modeling results, while emission trends, including carbon-related and nitrogen-based species, were evaluated using numerical predictions.

All results were analyzed comparatively between single-fuel B100 and dual-fuel $NH_3$–B100 operation to assess the performance–emission trade-offs associated with ammonia utilization.

## III. Results and Discussion

This chapter presents the results and discussion of the study, which are structured into five main sections: model validation, combustion characteristics, emission behavior, engine performance, and overall discussion. Model validation is performed by comparing the numerical simulation results with experimental data to assess the accuracy of the developed model. Combustion and emission characteristics are primarily analyzed using ANSYS Forte, while engine performance parameters are evaluated through a one-way coupling approach between ANSYS Forte and MATLAB. The discussion section integrates the findings from combustion, emissions, and performance analyses to provide a comprehensive interpretation of the results prior to the final conclusions.

3.1. Model Validation under Single-Fuel B100 Operation

The numerical model was first validated against experimental measurements of the baseline single-fuel B100 engine to ensure prediction reliability. Figure 3 compares the simulated and experimental brake power and torque across the tested engine speeds. Overall, the simulation results show good agreement with experiments, with deviations generally below 0.12–5.9% for power. The maximum prediction error was observed at 1400 rpm, corresponding to 5.95% for power. These discrepancies are considered acceptable for engine performance simulations and may be attributed to uncertainties in friction loss estimation, heat transfer modeling, and measurement tolerances. Therefore, the

validated model is deemed sufficiently accurate for subsequent dual-fuel combustion analysis

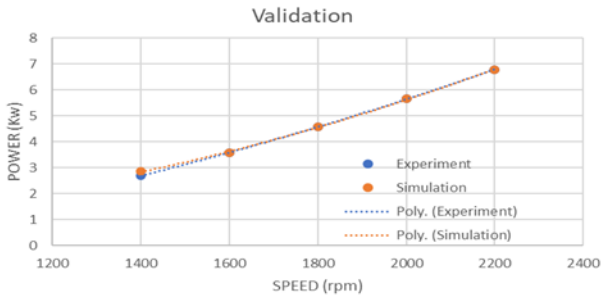


**Figure 3.** Comparison between Simulation and Experiment

3.2 Combustion Process

3.2.1. Comparison of In-Cylinder Pressure Profiles between Single-Fuel and Dual-Fuel Operation

Figures 4 and 5 present the in-cylinder pressure traces of the B100 single-fuel and $NH_3$–B100 dual-fuel (DF) combustion modes at various engine speeds. A clear distinction in both peak pressure magnitude and combustion phasing is observed between the two operating strategies.

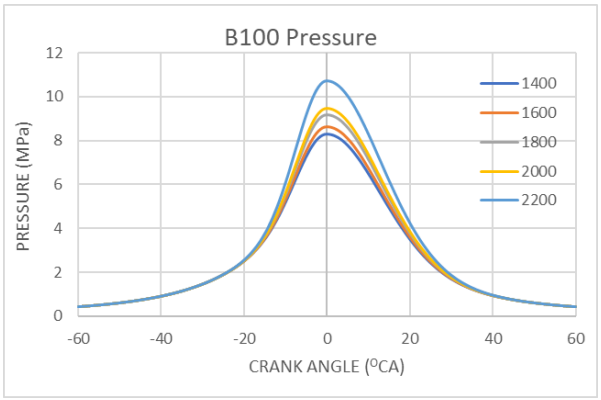


**Figure 4.** B100's Pressure vs Crank Angle Degree

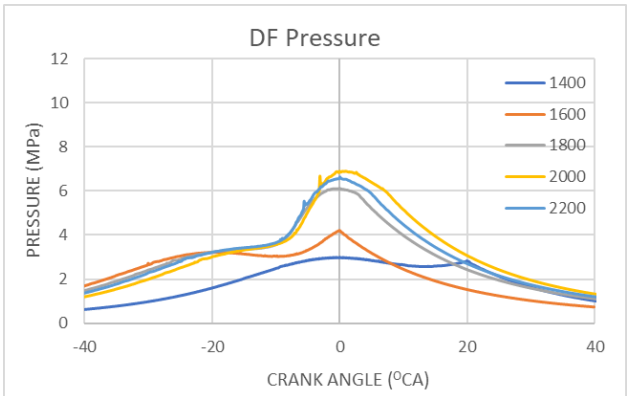


**Figure 5.** Dual-Fuel's Pressure vs Crank Angle Degree

Under B100 operation, the peak pressure increase consistently with engine speed, rising from approximately 8.28 MPa at 1400 rpm to 10.7 MPa at 2200 rpm. The pressure peaks occur close to top dead center (TDC), indicating rapid premixed combustion and efficient heat release. This behavior reflects the high reactivity and faster flame propagation of biodiesel, which promotes earlier combustion phasing and stronger pressure development near TDC.

In contrast, the $NH_3$–B100 dual-fuel mode exhibits significantly lower peak pressures across all speeds. The maximum pressure only reaches around 6.6–6.9 MPa at higher speeds, while at low speed (1400 rpm) it drops to approximately 3 MPa. Moreover, combustion phasing is noticeably retarded, as indicated by the shift of CA50 from about 9° ATDC in B100 to roughly 15° ATDC in DF operation. This delay is primarily attributed to the poor flammability, high ignition temperature, and slow flame speed of ammonia, which prolong the main heat-release process even though ignition is initiated by the biodiesel pilot.

The broader and staged pressure rise observed in DF operation suggests a two-stage combustion mechanism: early ignition from the B100 pilot followed by slower ammonia oxidation. This results in a smoother pressure gradient and reduced peak pressure compared to the single-fuel case.

From a performance perspective, the lower peak pressure and delayed combustion in DF operation indicate reduced indicated work and potentially lower thermal efficiency. However, the moderated pressure rise rate may also mitigate mechanical stress and combustion noise. In terms of emissions, the reduced peak temperature associated with lower pressure can suppress thermal $NO_x$ formation, whereas incomplete ammonia oxidation may increase unburned species such as $NH_3$ slip and UHC.

3.2.2 Temperature Distribution

The in-cylinder temperature history clearly distinguishes the combustion characteristics between single-fuel B100 and dual-fuel $NH_3$–B100 operation. For B100, the peak temperature remains consistently high and stable across the investigated speeds, reaching approximately 2500–2600 K (see Figure 6 for B100). The temperature curve is relatively symmetric around TDC, indicating that most of the heat release occurs near the beginning of the expansion stroke. This behavior suggests rapid ignition, short combustion duration, and more complete combustion, which are typical of conventional diesel-like fuels with high reactivity.

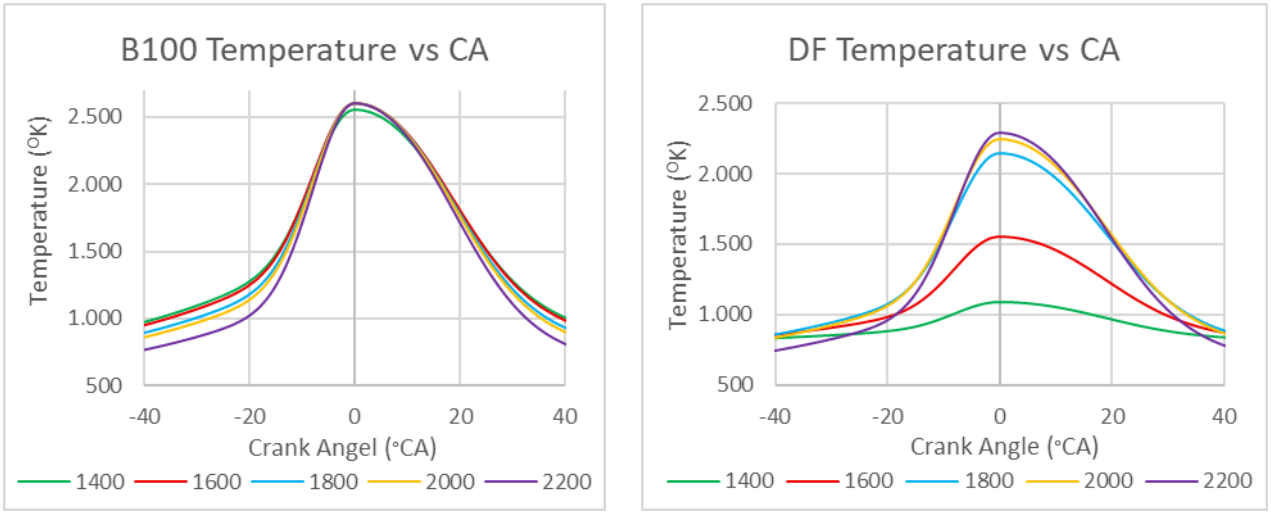


**Figure 6.** Temperature vs CA degree of B100 and Dual-Fuel (NH3-B100)

In contrast, the dual-fuel mode exhibits significantly lower peak temperatures and a stronger dependence on engine speed. The maximum temperature increases from approximately 1087 K at 1400 rpm to 2243.7 K at 2000 rpm, before slightly decreasing at 2200 rpm (see Figure 6 for BF). The temperature reduction at high speed is attributed to shorter residence time and incomplete energy release within the available crank-angle duration. This lower-temperature combustion environment is mainly associated with the slow flame speed and poor reactivity of ammonia, which delays heat release and limits peak thermal intensity.

From an emissions perspective, the reduced peak temperature under dual-fuel operation is expected to suppress thermal $NO_x$ formation, whereas incomplete combustion at low and high speeds may promote higher UHC, CO, and ammonia slip.

3.2.3 Heat Release Rate

The heat release rate profiles further confirm the differences in combustion dynamics between both fuels. The B100 HRR curves follow a typical diesel combustion pattern, characterized by ignition near −10°CA, a rapid premixed spike around TDC, and a gradual decay during the early expansion stroke (see Figure 7 for B100). The peak HRR increases with engine speed, from 64.66 J/deg at 1400 rpm to above 110 J/deg at 2200 rpm, indicating intensified combustion due to improved atomization, mixing, and turbulence at higher rotational speeds.

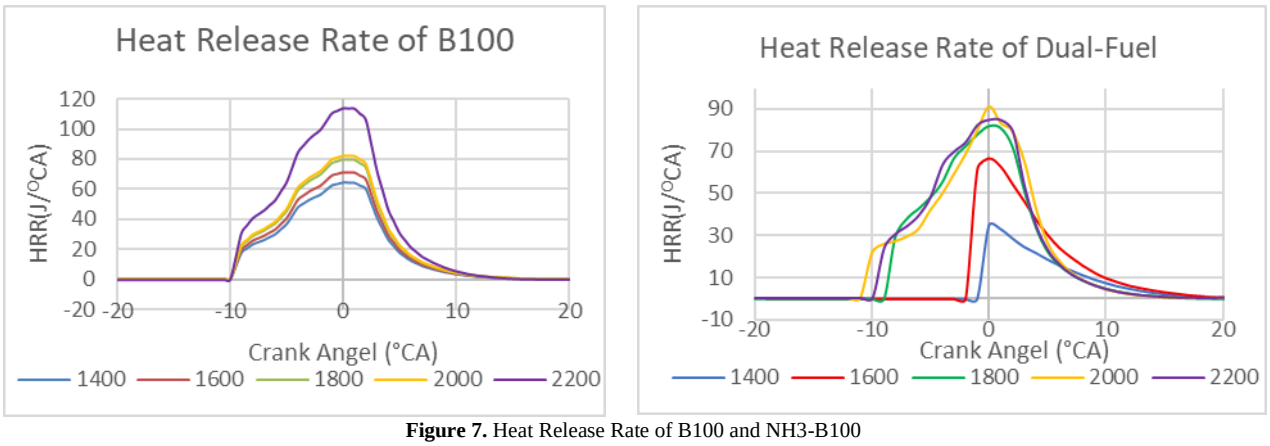


**Figure 7.** Heat Release Rate of B100 and NH3-B100

The peak HRR For the $NH_3$–B100 dual-fuel case, a single dominant premixed peak is observed close to TDC for all speeds (see Figure 7 for DF). The peak HRR increases progressively from 35.03 J/deg at 1400 rpm to 91.40 J/deg at 2000 rpm, before slightly decreasing at 2200 rpm. This trend reflects the competing effects between enhanced turbulence (which accelerates combustion) and reduced reaction time at very high speed. The lower HRR magnitude at low speeds indicates delayed ignition and slower chemical kinetics of ammonia, while the reduced peak at 2200 rpm suggests incomplete combustion due to shortened residence time.

The HRR characteristics imply that B100 combustion is dominated by diffusion-controlled burning with high energy density, whereas the $NH_3$–B100 system is primarily premixed-controlled and kinetically limited. Consequently, dual-fuel operation produces smoother and lower-intensity heat release, which reduces peak pressure and temperature but may compromise combustion completeness.

3.3 Emissions

The emission characteristics distinguishing B100 single-fuel operation from ammonia–B100 dual-fuel combustion primarily include nitrogen oxides ($NO_x$), carbon monoxide (CO), and ammonia slip ($NH_3$ slip). Carbon dioxide ($CO_2$) emissions are also considered, as the ammonia-B100 dual fuel configuration still involves carbon-containing fuel. However, in this study, particular attention is given to CO emissions and $NH_3$ slip, as these parameters are closely associated with combustion instability and the potential occurrence of misfire under ammonia-B100 dual fuel operation.

3.3.1. NOx Emissions and Their Relationship to the Combustion Process

Figures 8 and 9 present the specific $NO_x$ emissions (g/kWh) of both B100 single-fuel and dual-fuel $NH_3$–B100 operation over the engine speed range of 1400–2200 rpm. For both fuels, the specific $NO_x$ emissions consistently decrease as engine load increases. This trend is primarily attributed to the normalization effect of brake-specific emissions, where low brake power at light load results in higher specific values, even if the absolute $NO_x$ mass is relatively small.

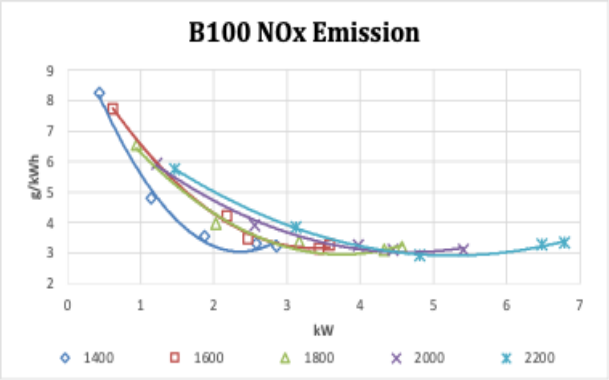


**Figure 8**. $NO_X$ emission of B100

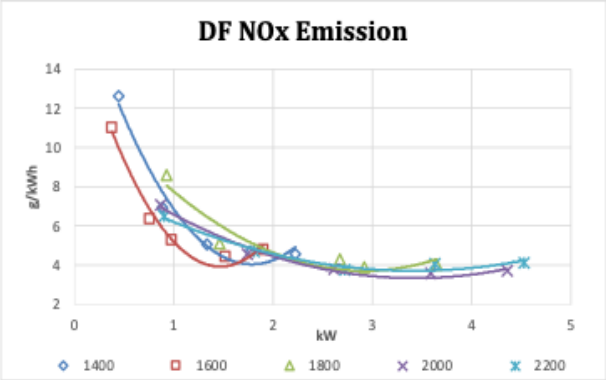


**Figure 9**. $NO_X$ emission of dual fuels $NH_3$-B100

Under B100 single-fuel operation, the highest $NO_x$ levels occur at 20% load, reaching approximately 8.26 g/kWh at 1400 rpm and gradually decreasing with increasing speed. As the load increases to 40–60%, $NO_x$ declines to around 3.4–4.0 g/kWh and further stabilizes near 3.1–3.3 g/kWh at 80–100% load. This behavior is consistent with typical diesel combustion, where higher loads improve combustion efficiency and reduce the influence of normalization. Additionally, the inherent oxygen content of biodiesel promotes more complete oxidation and locally higher flame temperatures, which can favor thermal $NO_x$ formation, particularly under lean combustion regions.

In contrast, the dual-fuel $NH_3$–B100 configuration exhibits substantially higher $NO_x$ emissions at low load, with values exceeding 12 g/kWh at 1400 rpm and remaining noticeably above those of B100 across all speeds. This elevated $NO_x$ is associated with two main mechanisms. First, the same low-power normalization effect amplifies the specific emissions. Second, ammonia introduces fuel-bound nitrogen, which contributes directly to $NO_x$ formation through fuel-N pathways in addition to conventional thermal $NO_x$ mechanisms. As the load increases, the specific $NO_x$ decreases significantly to approximately 5.0–5.4 g/kWh at medium load and stabilizes around 3.8–4.7 g/kWh at high load, where the increasing brake power growth rate becomes larger than the $NO_x$ formation rate.

When correlated with the combustion analysis, the results indicate that although the dual-fuel mode generally produces lower peak temperatures and smoother heat release, the presence of chemically bound nitrogen in ammonia offsets the expected thermal $NO_x$ reduction. Consequently, fuel-$NO_x$ becomes the dominant contributor in the $NH_3$–B100 case. This explains why $NO_x$ emissions remain higher in dual-fuel operation despite the lower in-cylinder temperature compared to B100.

Overall, the findings suggest that while ammonia substitution effectively reduces carbon-based emissions, additional $NO_x$ mitigation strategies—such as injection timing optimization, ammonia energy fraction control, or after-treatment systems—are required to balance the trade-off between decarbonization and nitrogen-oxide formation.

3.3.2 $CO_2$ Emission Characteristics

Figures 10 and 11 illustrate the variation of brake-specific $CO_2$ emissions (g/kWh) for both B100 single-fuel and dual-fuel $NH_3$–B100 operation over the speed range of 1400–2200 rpm. For both fueling modes, $CO_2$ emissions consistently decrease with increasing engine load. This behavior is primarily associated with a brake-specific normalization effect and improved combustion efficiency at higher loads. As the brake power increases, more useful work is produced per unit of fuel energy, resulting in lower $CO_2$ emissions per kWh, even though the absolute fuel consumption may rise.

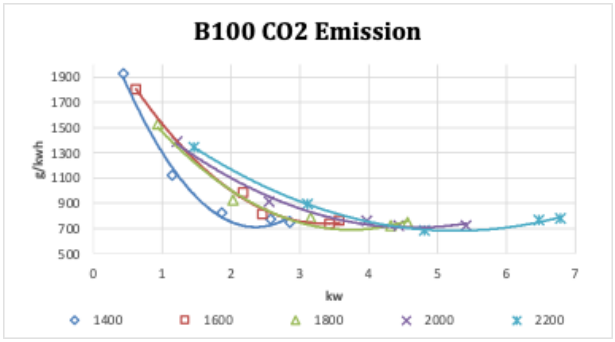


**Figure 10.** B100 CO2 Emission

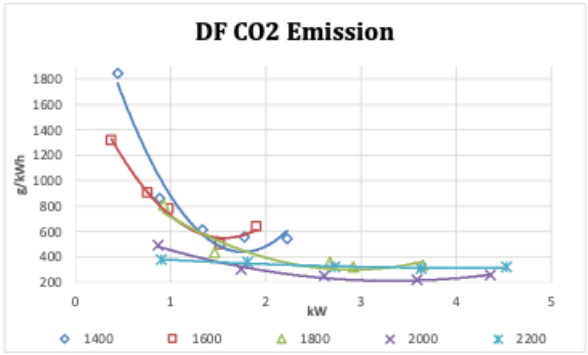


**Figure 11.** Dual Fuel CO2 Emission

Under B100 single-fuel operation, the highest $CO_2$ emissions are observed at light load (20%), reaching approximately 1900 g/kWh at 1400 rpm and gradually decreasing with increasing speed. A sharp reduction occurs at medium loads (40–60%), where $CO_2$ drops to around 700–1100 g/kWh, followed by stabilization at approximately 720–780 g/kWh at high loads (80–100%). This trend reflects improved thermal efficiency and more complete energy conversion as the engine operates closer to its optimal load range.

In contrast, the dual-fuel $NH_3$–B100 mode exhibits the same decreasing trend with load but with significantly lower $CO_2$ levels across all operating conditions. At high speed and high load, $CO_2$ emissions are substantially reduced, reaching approximately 380–430 g/kWh at 1800–2200 rpm and around 300 g/kWh at 1400–1600 rpm. The pronounced reduction relative to B100 is primarily attributed to carbon substitution. Since ammonia contains no carbon, its combustion does not directly produce $CO_2$. Consequently, replacing a portion of the biodiesel energy with ammonia proportionally lowers the overall carbon input to the engine. This observation is consistent with the adopted pilot-energy strategy, where only a limited fraction of B100 is used for ignition, thereby reducing the total carbon-based emissions.

Overall, the results confirm that ammonia substitution is highly effective for decarbonization, enabling substantial reductions in brake-specific $CO_2$ emissions while maintaining stable engine performance. These findings highlight the potential of $NH_3$–B100 dual-fuel operation as a viable pathway toward low-carbon or near-zero-carbon marine engine applications

### 3.3.3 Carbon Monoxide (CO) Emission Characteristics

Figures 12 and 13 present the brake-specific carbon monoxide (CO) emissions for both B100 single-fuel and $NH_3$–B100 dual-fuel operation over the investigated speed and load range. In general, CO emissions exhibit a strong dependence on engine load, indicating that combustion completeness improves as the engine transitions from low to medium–high load conditions.

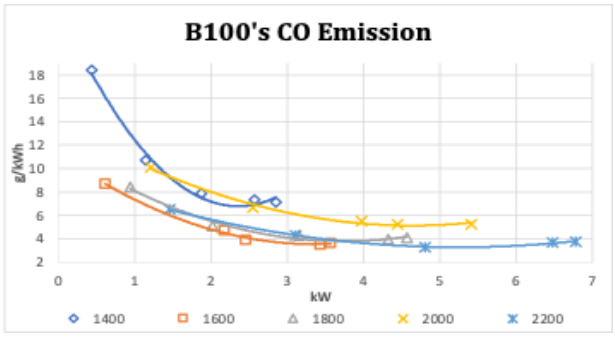


**Figure 12.** CO emission of B100

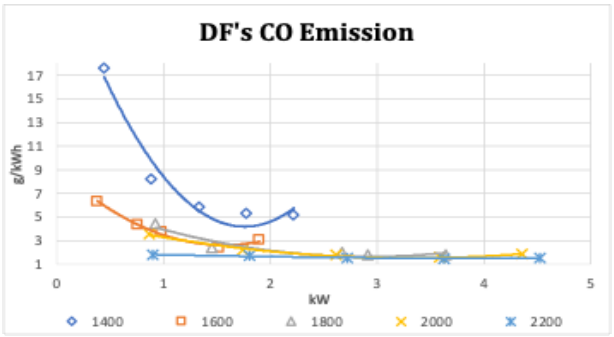


**Figure 13.** CO emission of dual fuel $NH_3$-B100

For B100 single-fuel operation (Fig. 12), CO emissions range from 3.306 to 18.418 g/kWh, with the highest value observed at 1400 rpm and 20% load and the lowest at 2200 rpm and 60% load. Increasing the load from 20% to 100% consistently reduces CO at all speeds (e.g., 18.418 to 7.154 g/kWh at 1400 rpm and 6.500 to 3.754 g/kWh at 2200 rpm). This behavior is primarily attributed to improved combustion conditions at higher loads. Low-load operation is characterized by lower in-cylinder and exhaust temperatures, longer ignition delays, and slower CO-to-$CO_2$ oxidation kinetics, which limit complete oxidation and promote higher CO formation. Conversely, higher loads elevate combustion temperature and reaction rates, enhancing oxidation efficiency and reducing residual CO. A slight increase in CO at very high loads (80–100%) is observed in several cases, suggesting the formation of locally rich zones or mixing limitations that restrict complete oxidation.

Under $NH_3$–B100 dual-fuel operation (Fig. 13), CO emissions remain load-dependent but are generally lower than those of B100 across most operating points, ranging from 1.494 to 17.573 g/kWh. At 1400 rpm, CO decreases monotonically with increasing load (17.573 to 5.153 g/kWh). At higher speeds, CO decreases until approximately 80% load, followed by a slight rebound at

full load, likely due to local mixture stratification or oxidation constraints similar to those observed in single-fuel operation. Notably, at 2200 rpm, CO levels remain consistently low throughout the entire load range, reaching a minimum of 1.494 g/kWh at 80% load.

A direct comparison at 2200 rpm confirms the advantage of dual-fuel operation, where CO emissions are substantially lower than B100-only combustion at all loads, with reductions of 52–72% and an average decrease of approximately 62%. This improvement is mechanistically consistent with the carbon-free nature of ammonia. Since $NH_3$ does not contain carbon, CO formation primarily originates from the limited B100 pilot fraction, thereby reducing the overall carbon available for incomplete oxidation. Consequently, ammonia substitution effectively suppresses CO formation while maintaining stable combustion performance.

Overall, the results demonstrate that dual-fuel $NH_3$–B100 operation provides a clear benefit in reducing incomplete-combustion emissions, particularly CO, and supports the potential of ammonia-based strategies for cleaner and lower-carbon engine operation.

### 3.3.4 UHC and Ammonia Slip Emissions

Figures 14–15 illustrate the trends of unburned hydrocarbon (UHC) emissions for both fueling modes and ammonia slip for the dual-fuel configuration. In general, incomplete-combustion emissions exhibit strong load dependence, reflecting improvements in oxidation efficiency as combustion temperature and in-cylinder reaction rates increase with engine load.

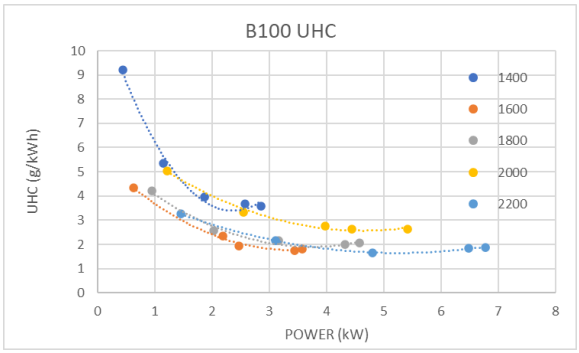


**Figure 14** UHC emission of B100

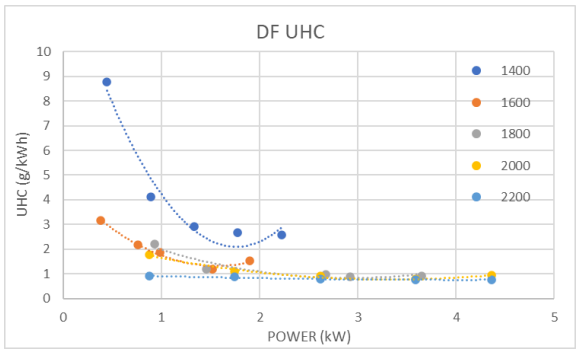


**Figure 15.** UHC emission dual fuel of $NH_3$-B100

For B100 single-fuel operation (Fig. 14), UHC emissions decrease markedly with increasing load, spanning 1.65-9.2 g/kWh across all engine speeds. The highest UHC value is observed at 1400 rpm and 20% load (9.20 g/kWh), while the lowest occurs at 2200 rpm and 60% load (1.653 g/kWh). Increasing load from 20% to 100% produces substantial reductions (e.g., 9.2 to 3.58 g/kWh at 1400 rpm and 3.25 to 1.87 g/kWh at 2200 rpm). This behavior is consistent with low-load combustion being more susceptible to incomplete oxidation, wall-quenching effects, and lower in-cylinder temperatures, which inhibit the complete breakdown of fuel hydrocarbons. At higher loads, elevated temperatures and improved turbulent mixing enhance oxidation kinetics, thereby reducing residual hydrocarbons. Minor rebounds near full load are occasionally observed, indicating localized rich zones and mixing-oxidation limitations under high fueling rates.

Under $NH_3$–B100 dual-fuel operation (Fig. 15), UHC emissions are generally lower and more stable, ranging from 0.75 to 8.79 g/kWh. The maximum occurs at 1400 rpm and 20% load (8.79 g/kWh), while the minimum is recorded at 2200 rpm and 80% load (0.75 g/kWh). Similar to single-fuel operation, UHC decreases with increasing load and then approaches a plateau or slight rebound near full load. Because ammonia contains no carbon, UHC formation in dual-fuel mode originates primarily from the B100 pilot fraction and its oxidation completeness. Consequently, reduced carbon input combined with improved high-temperature oxidation leads to consistently lower UHC levels compared to B100-only combustion.

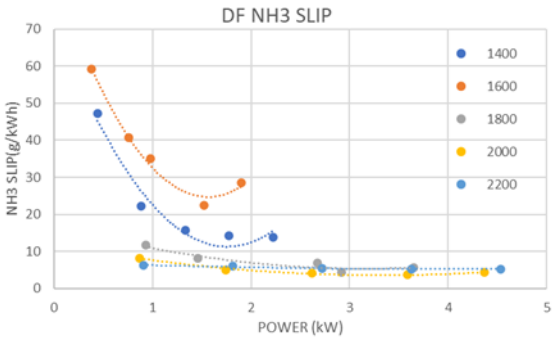


**Figure 16.** $NH_3$ Slip

In addition to UHC, ammonia slip becomes a characteristic emission for dual-fuel operation (Fig. 16). $NH_3$ slip decreases significantly with increasing load at all speeds. At 20% load, slip is highest, particularly at low-mid speeds (approximately 47 g/kWh at 1400 rpm and 59 g/kWh at 1600 rpm), whereas substantially lower values are observed at higher speeds (approximately 7-12 g/kWh). As load increases to 40–60%, $NH_3$ slip drops sharply and stabilizes at relatively low levels of about 4-6 g/kWh at 60-100% load. This trend indicates enhanced ammonia oxidation under higher load conditions, driven by increased in-cylinder temperature, stronger turbulence, and more effective ignition support from the pilot fuel. Conversely, low-load operation promotes incomplete ammonia conversion, resulting in greater unreacted $NH_3$ in the exhaust, a behavior widely reported in ammonia dual-fuel combustion systems.

A clear correlation can be identified between UHC and $NH_3$ slip trends. Both emissions represent incomplete-combustion products and therefore decrease simultaneously as combustion temperature and oxidation efficiency improve with load. However, while UHC is associated with carbon-based fuel fragments from the biodiesel pilot, $NH_3$ slip reflects incomplete oxidation of nitrogen-based fuel. This trade-off highlights a key challenge of ammonia dual-fuel engines: although carbon-related emissions (CO, $CO_2$, and UHC) are reduced, ammonia slip may increase under suboptimal combustion conditions. Therefore, optimizing pilot fraction, injection timing, and ammonia phasing is essential to ensure complete oxidation and minimize both hydrocarbon and ammonia-related emissions.

Overall, the results demonstrate that dual-fuel $NH_3$-B100 operation effectively lowers carbon-based incomplete-combustion emissions while introducing ammonia slip as a new emission pathway, emphasizing the need for careful combustion control and injection strategy optimization.

Overall, the comparative emission analysis reveals clear combustion-dependent trade-offs between B100 single-fuel and $NH_3$-B100 dual-fuel operation across the tested speed and load range. Increasing engine load consistently improves combustion completeness, resulting in lower brake-specific emissions of CO, UHC, and $NH_3$ slip for both modes due to higher in-cylinder temperatures, enhanced oxidation kinetics, and stronger turbulence intensity. In the dual-fuel configuration, the substitution of carbon-based biodiesel with carbon-free ammonia significantly reduces carbon-related emissions, particularly $CO_2$, CO, and UHC, confirming the effectiveness of ammonia in suppressing carbon formation pathways. However, this carbon reduction benefit is accompanied by new nitrogen-related challenges. The presence of fuel-bound nitrogen in ammonia promotes higher $NO_x$ formation through thermal and fuel-N mechanisms and introduces $NH_3$ slip under low-load or low-temperature conditions, indicating incomplete ammonia oxidation. Consequently, while $NH_3$-B100 dual-fuel combustion demonstrates strong potential for near-zero carbon emissions, achieving an optimal balance between efficiency and emissions requires careful control of combustion phasing, pilot fuel fraction, and injection strategy. These findings highlight that emission performance in ammonia-based dual-fuel engines is governed primarily by combustion temperature and oxidation completeness, making combustion optimization the key pathway for simultaneously minimizing carbon- and nitrogen-related pollutants. Therefore, the dual-fuel $NH_3$–B100 strategy offers a promising pathway toward low-carbon marine propulsion, provided that combustion control techniques are applied to mitigate $NO_x$ formation and ammonia slip.

### 3.4 Engine Performance

The indicated mean effective pressure (IMEP) obtained from the ANSYS Forte simulations was used as the primary combustion output for engine performance evaluation. Mechanical losses were accounted for by estimating the friction mean effective pressure (FMEP) using empirical correlations as a function of engine speed. The calculated IMEP and FMEP values were subsequently coupled in a one-way manner with a MATLAB-based 1D performance model to determine brake-related performance parameters. This approach allows the integration of detailed combustion analysis with overall engine performance evaluation while maintaining reasonable computational efficiency.

Table 2 presents the indicated mean effective pressure (IMEP) obtained from ANSYS Forte simulations and the corresponding friction mean effective pressure (FMEP) calculated using empirical correlations at various engine operating conditions. The IMEP values represent the net combustion work predicted from the 3D in-cylinder combustion simulations, while the FMEP accounts for mechanical losses associated with engine friction.

The IMEP values obtained from the ANSYS Forte simulations were used as the primary combustion output to represent in-cylinder work under both single-fuel and dual-fuel operating conditions. Mechanical losses were incorporated by estimating the friction mean effective pressure (FMEP) using established empirical correlations as a function of engine speed. The combination of IMEP and FMEP was subsequently employed in a one-way coupling framework with a MATLAB-based 1D performance model to determine brake-related performance parameters. This approach enables the integration of detailed combustion analysis with overall engine performance evaluation while maintaining computational efficiency.

#### 3.4.1 Specific Fuel Oil Consumption (SFOC) Characteristics

Figures 17 and 18 present the specific fuel oil consumption (SFOC) for the engine operating under single fuel B100 and dual-fuel $NH_3$-B100 conditions, respectively. For the B100 single-fuel operation (Figure 17), SFOC generally decreases with increasing engine speed, indicating improved fuel utilization efficiency at higher operating speeds. This trend is consistent with enhanced combustion completeness and reduced relative friction losses as engine speed increases

TABLE 2.
IMEP AND FMEP VALUE USED FOR 3D-1D COUPLING ANALYSIS

| Fuel | RPMs | Load | IMEP | FMEP | Fuel | RPMs | Load | IMEP | FMEP |
|---|---|---|---|---|---|---|---|---|---|
| B100 | 1400 | 20 | 0,1658 | 0,09 | NH3-B100 | 1400 | 20 | 0,16755 | 0,09 |
| | | 40 | 0,2888 | 0,09 | | | 40 | 0,24469 | 0,09 |
| | | 60 | 0,41536 | 0,09 | | | 60 | 0,32184 | 0,09 |
| | | 80 | 0,537314 | 0,09 | | | 80 | 0,39898 | 0,09 |
| | | 100 | 0,58638 | 0,09 | | | 100 | 0,47612 | 0,09 |
| | 1600 | 20 | 0,197639 | 0,103 | | 1600 | 20 | 0,14528 | 0,103 |
| | | 40 | 0,43468 | 0,103 | | | 40 | 0,18726 | 0,103 |
| | | 60 | 0,47725 | 0,103 | | | 60 | 0,21187 | 0,103 |
| | | 80 | 0,6251 | 0,103 | | | 80 | 0,27124 | 0,103 |
| | | 100 | 0,646 | 0,103 | | | 100 | 0,31322 | 0,103 |
| | 1800 | 20 | 0,2432 | 0,116 | | 1800 | 20 | 0,24172 | 0,116 |
| | | 40 | 0,3896 | 0,116 | | | 40 | 0,31325 | 0,116 |
| | | 60 | 0,5423 | 0,116 | | | 60 | 0,4771 | 0,116 |
| | | 80 | 0,6992 | 0,116 | | | 80 | 0,5103 | 0,116 |
| | | 100 | 0,7332 | 0,116 | | | 100 | 0,60882 | 0,116 |
| | 2000 | 20 | 0,2769 | 0,129 | | 2000 | 20 | 0,23514 | 0,129 |
| | | 40 | 0,439 | 0,129 | | | 40 | 0,3412 | 0,129 |
| | | 60 | 0,6116 | 0,129 | | | 60 | 0,44726 | 0,129 |
| | | 80 | 0,66904 | 0,129 | | | 80 | 0,565345 | 0,129 |
| | | 100 | 0,7865 | 0,129 | | | 100 | 0,65938 | 0,129 |
| | 2200 | 20 | 0, 44032 | 0,142 | | 2200 | 20 | 0,2421 | 0,142 |
| | | 40 | 0,5485 | 0,142 | | | 40 | 0,3421 | 0,142 |
| | | 60 | 0,67139 | 0,142 | | | 60 | 0,4426 | 0,142 |
| | | 80 | 0,85762 | 0,142 | | | 80 | 0,5428 | 0,142 |
| | | 100 | 0,98912 | 0,142 | | | 100 | 0,64259 | 0,142 |

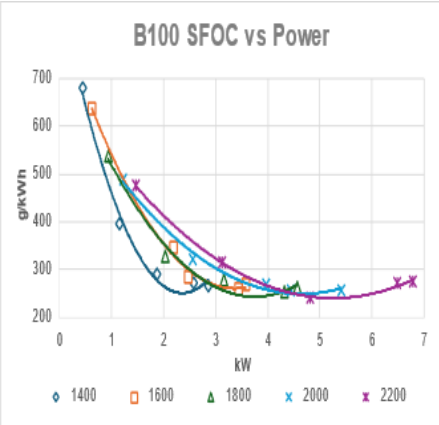


**Figure 17.** Specific fuel consumption of B100

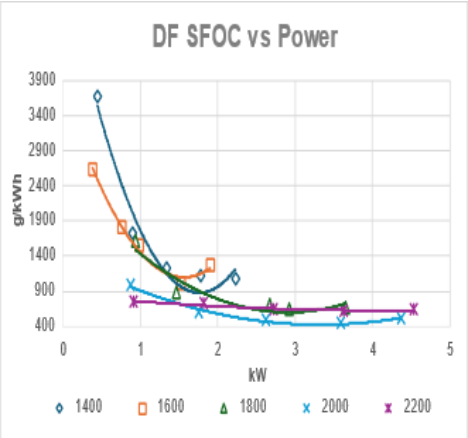


**Figure 18.** Specific fuel consumption of dual fuel $NH_3$-B100

Under dual fuel $NH_3$-B100 operation (Figure 18), a different SFOC behavior is observed. The SFOC values tend to increase compared to single-fuel B100 operation, particularly at low and medium engine speeds. This increase can be attributed to the altered combustion characteristics introduced by ammonia addition, including delayed combustion phasing, reduced peak heat release rate, and slower oxidation kinetics. These factors reduce the effective conversion of fuel energy into useful work, thereby increasing the fuel consumption per unit power output.

At higher engine speeds, the difference in SFOC between single-fuel and dual-fuel operation becomes less pronounced. This behavior is associated with higher in-cylinder temperatures and enhanced turbulence intensity, which promote more effective combustion and partially compensate for the lower reactivity of ammonia. Nevertheless, the overall SFOC results indicate that while ammonia substitution offers advantages in reducing carbon-related emissions, it introduces efficiency penalties that must be addressed through optimization of ammonia energy fraction and combustion strategy.

### 3.4.2 Power and Torque

Figures 19 and 20 present the brake power and torque characteristics of the engine under single-fuel B100 and dual fuel $NH_3$-B100 operating conditions. In general, both operating modes exhibit the expected trend of increasing power and torque with engine speed due to higher combustion frequency and greater total energy release per unit time.

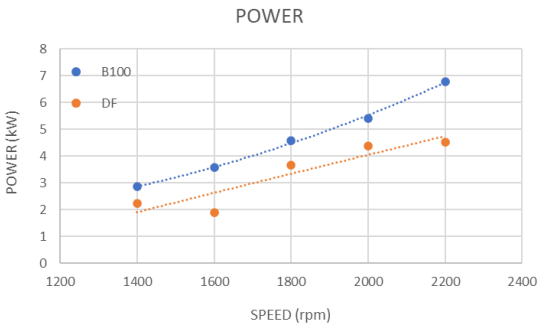


**Figure 19.** Comparison Power between B100 and dual fuel NH3-B100

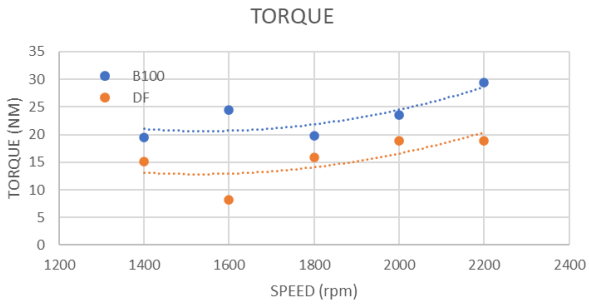


**Figure 20.** Comparison torque between B100 and dual fuel NH3-B100

For the single-fuel B100 case, the engine demonstrates stable and higher brake power and torque outputs across the investigated speed range. This behavior is attributed to the favorable combustion properties of biodiesel, including its relatively high cetane number and inherent oxygen content, which promote rapid ignition and efficient heat release. The sharper heat release rate and higher peak in-cylinder pressure observed in the combustion analysis contribute directly to greater indicated work and consequently higher brake output.

In contrast, the dual-fuel $NH_3$–B100 operation shows a slight reduction in both power and torque compared to the single-fuel baseline, particularly at lower and medium engine speeds. The decrease is primarily associated with the slower combustion kinetics of ammonia, characterized by delayed ignition, reduced peak heat release rate, and lower in-cylinder pressure development. These effects diminish the indicated mean effective pressure (IMEP), which subsequently reduces the brake mean effective pressure after accounting for mechanical losses. As a result, the overall power conversion efficiency decreases under higher ammonia substitution ratios.

At higher engine speeds, however, the gap in power and torque between the two modes becomes smaller. Increased turbulence intensity and elevated in-cylinder temperatures enhance combustion rates and partially compensate for ammonia's lower reactivity, enabling more complete energy release. This behavior indicates that the dual-fuel strategy can maintain acceptable engine output at higher speeds despite the inherent combustion limitations of ammonia.

Overall, the power and torque results confirm that while ammonia substitution contributes to lower carbon emissions, it introduces moderate penalties in engine output, particularly at low-speed operation. These trade-offs highlight the importance of optimizing ammonia energy fraction and injection strategy to balance performance and emission objectives.

## 3.5 Discussion

### 3.5.1 Combustion behaviour

The combustion characteristics at low (1400 rpm) and high (2200 rpm) engine speeds for both single-fuel B100 and dual-fuel $NH_3$-B100 operation are illustrated through the in-cylinder pressure, temperature, and heat release rate (HRR) profiles, as shown in Figures 21–23. These parameters provide complementary insight into combustion intensity, heat release dynamics, and thermal conditions inside the cylinder.

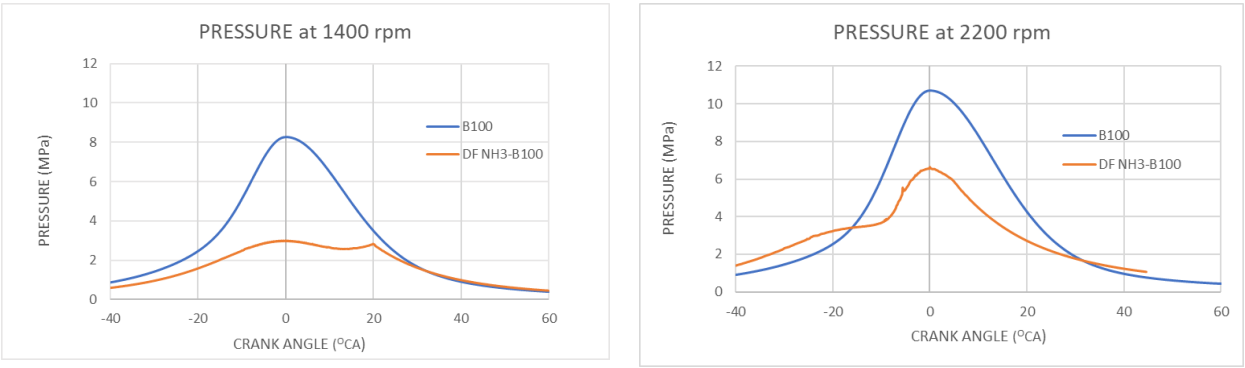


**Figure 21** Difference In Pressure Trend Between Single Fuel B100 And Dual Fuel NH3-B100 At 1400 And 2200 Rpm

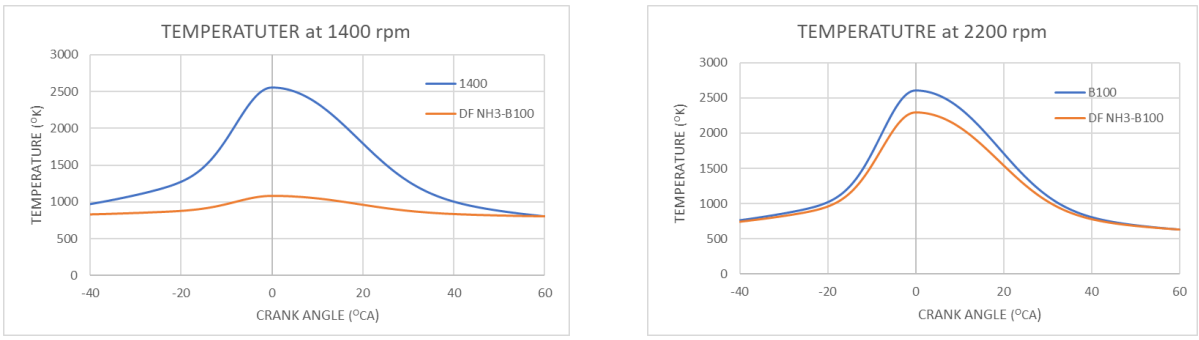


**Figure 22** Difference In Temperature Trends Between B100 Single Fuel And NH3-B100 Dual Fuel At 1400 And 2200 Rpm

At low engine speed (1400 rpm), the performance gap between single-fuel B100 and $NH_3$–B100 dual-fuel (DF) combustion is most pronounced. Ammonia combustion is inherently characterized by poor ignitability, low laminar burning velocity, and slow chemical kinetics, which extend the heat-release duration and suppress the instantaneous pressure rise rate [4], [5]. Consequently, the DF mode exhibits lower peak heat release and weaker in-cylinder pressure–temperature development [23], [25]. In this study, the peak HRR under DF reaches only 35.03 J/deg at 1400 rpm and 66.77 J/deg at 1600 rpm, substantially below the corresponding B100 values (e.g., 64.66 J/deg at 1400 rpm). Such behavior indicates kinetically limited combustion and incomplete energy conversion at low speed [8], [22].

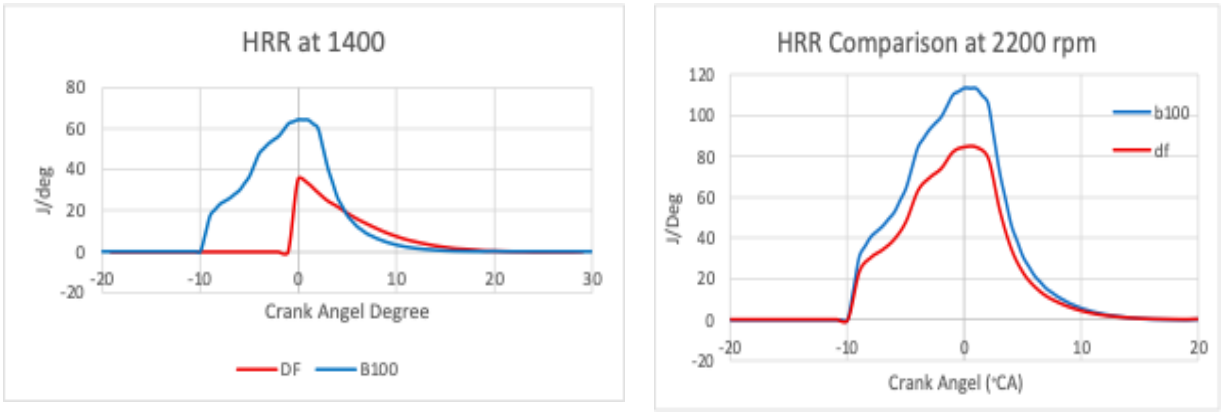


**Figure 23**. Difference In HRR Trends Between B100 Single Fuel And NH3-B100 Dual Fuel At 1400 And 2200 Rpm

This trend is consistent with previous pilot-ignited ammonia studies, where increasing the ammonia share broadens the heat-release rate, strengthens late burning/afterburning, and reduces peak pressure compared with diesel-like combustion, particularly under marginal temperature conditions [27]. Moreover, stable ignition in ammonia DF engines strongly depends on the pilot injection strategy, since the pilot controls early kernel formation and the rapid combustion fraction, which directly affects IMEP stability and emissions [28].

When the engine speed increases to 2000–2200 rpm, the combustion regime shifts toward higher temperature and enhanced turbulence. Faster air–fuel mixing and improved transport processes accelerate ammonia oxidation despite the shorter available cycle time. As a result, DF combustion becomes more developed, with the peak HRR rising to 84.75 J/deg at 2200 rpm, although still lower than B100 (114.6 J/deg).

The improved combustion intensity at high speed explains the reduced ignition delay, higher pressure traces, and narrower performance gap between DF and B100. Similar improvements in ammonia conversion at elevated speed/load have been widely reported in experimental investigations [29], [30].

### 3.5.2 Emission implications

The emission behavior follows the same thermochemical mechanism. Dual-fuel operation significantly reduces carbon-based emissions because a large portion of the supplied energy originates from carbon-free ammonia. Consequently, brake-specific $CO_2$ emissions decrease markedly under DF conditions [24]. At high load (1800–2200 rpm), DF $CO_2$ levels are limited to approximately 309–489 g/kWh, which are substantially lower than those of B100 (≈700–1500 g/kWh), demonstrating the effectiveness of ammonia substitution for decarbonization.

Carbon-related incomplete combustion products are also suppressed [23], [24]. At 2200 rpm, DF operation achieves an average CO reduction of approximately 62% relative to B100, indicating that CO formation is primarily associated with the limited B100 pilot fraction. Similarly, UHC emissions are generally lower and more

stable under DF operation due to the absence of hydrocarbon content in ammonia.

However, the benefits in carbon reduction are accompanied by nitrogen-related trade-offs. NOx emissions under DF are slightly higher than those of B100 at several operating points (e.g., 6.468 vs. 5.76 g/kWh at 20% load and 2200 rpm; 4.04–4.11 vs. 3.29–3.30 g/kWh at full load). This increase is attributable to the fuel-bound nitrogen in ammonia and the elevated local combustion temperatures that promote thermal and fuel-NOx formation pathways. In addition, ammonia slip becomes significant under low-speed/low-load conditions, reaching approximately 47–59 g/kWh, but decreases sharply to 4.4–6.3 g/kWh at high load. This reduction reflects improved oxidation efficiency at higher in-cylinder temperatures and stronger turbulence. Similar trends have been widely reported in ammonia DF combustion studies, where unburned $NH_3$ decreases with increasing load and speed [31].

3.5.3 Performance implications

From a performance perspective, DF combustion remains less efficient than B100 across the entire operating range. The slower reaction rate and incomplete ammonia oxidation result in lower effective pressure, reduced brake power, and higher SFOC. Although the DF mode preserves the conventional torque-speed and power-speed characteristics of compression ignition engines, a persistent power penalty of approximately 0.8–1.2 kW is observed compared with B100.

Nevertheless, the performance deficit narrows at higher speeds (2000–2200 rpm), where improved mixing and faster chemical reactions enhance ammonia utilization. This operating region therefore represents a practical

DF window, balancing acceptable efficiency with substantial $CO_2$ reduction. Such findings indicate that ammonia-based DF engines are more suitable for medium-to-high load marine operation rather than low-load conditions [8,25].

3.5.4 Model capability and overall implication

Finally, the integrated ANSYS Forte–MATLAB workflow demonstrates good predictive capability in linking in-cylinder combustion phenomena to brake-level performance indicators. The simulated brake power shows close agreement with reference data, with errors ranging from 0.20–5.94%, confirming the reliability of the coupled 3D-1D framework. This validated platform enables systematic evaluation of combustion, performance, and emissions across the entire rpm–load map and provides a robust basis for further optimization, including pilot fraction adjustment, injection timing control, and operating-window selection. [19-21]

Overall, the results confirm that $NH_3$–B100 dual-fuel operation is technically feasible and offers substantial decarbonization potential. While combustion limitations at low speed remain challenging, operation at higher speed/load conditions significantly improves ammonia utilization and reduces carbon emissions, highlighting a clear pathway for practical implementation in marine diesel engines.

## IV. CONCLUSION

$NH_3$–B100 dual-fuel (DF) combustion is technically feasible but strongly speed-dependent. At low speeds (1400-1600 rpm), combustion remains kinetically and pilot-limited, resulting in lower heat-release intensity (35.03-66.77 J/deg) compared with B100 (64.66 J/deg), weaker pressure-temperature development, and slower energy release. As speed increases to 2000-2200 rpm, turbulence and in-cylinder temperature enhance ammonia oxidation, raising HRR to 84.75 J/deg and producing more stable and complete combustion, although still below B100 levels.

DF operation substantially reduces carbon-based emissions due to ammonia's carbon-free nature. $CO_2$ decreases markedly to approximately 309-489 g/kWh under high-load conditions, far below B100 (~700-1500 g/kWh), while CO emissions are reduced by about 62% on average. However, trade-offs include slightly higher NOx and notable $NH_3$ slip at low-load/low-speed operation (≈47-59 g/kWh), which diminishes significantly at higher load/speed (≈4-6 g/kWh) as combustion completeness improves.

In terms of brake performance, DF preserves the conventional CI engine trends but exhibits lower power/torque and higher SFOC than B100. The performance deficit is most pronounced at low speeds due to slow ammonia kinetics, whereas the gap narrows at medium-to-high load and 2000-2200 rpm, identifying this region as the practical operating window where efficiency penalties are minimized while emissions benefits are retained.

The integrated ANSYS Forte-MATLAB workflow effectively links combustion metrics (IMEP/FMEP and HRR) to brake-level outputs (BMEP, power, torque, and SFOC) and enables systematic emissions evaluation across the full rpm-load map. The good agreement with reference data (0.20-5.94% error) confirms the reliability of the framework for performance-emissions trade-off analysis and future optimization of pilot strategy and operating conditions.

## ACKNOWLEDGEMENTS

The authors would like to take this opportunity to express our gratitude to Mr. Nur Afandi, Assistant of the Marine Power and Propulsion Systems Laboratory, for his assistance in preparing the experiments and simulation equipment.

## REFERENCES

[1] *Strategy on Reduction of GHG Emissions from Ships*. London, U.K.: IMO, 2023.

[2] E. A. Bouman, E. Lindstad, A. I. Rialland, and A. H. Strømman, "State-of-the-art technologies, measures, and potential for reducing greenhouse gas emissions from shipping," *Renewable and Sustainable Energy Reviews*, vol. 52, pp. 408–421, 2017. https://doi.org/10.1016/j.trd.2017.03.022

[3] Smith, T., Raucci, C., Haji Hosseinloo S., Rojon I., Calleya J., Suárez de la Fuente S., Wu P., Palmer K. CO2 emissions from international shipping. Possible reduction targets and their

associated pathways. Prepared by UMAS, October 2016, London.

[4] A Valera-Medina, H Xiao, M Owen-Jones, W.I.F. David, P.J. Bowen., ," *Progress in Energy and Combustion Science*, vol. 69, pp. 63–102, 2018. https://doi.org/10.1016/j.pecs.2018.07.001

[5] H. Kobayashi, A. Hayakawa, K. D. Kunkuma, and E. C. Okafor, "Science and technology of ammonia combustion," *Proceedings of the Combustion Institute*, vol. 37, pp. 109–133, 2019. https://doi.org/10.1016/j.proci.2018.09.029

[6] Samuel Ronald Holden, Zhezi Zhang, Jian Gao, Junzhi Wu, Dongke Zhang., "Ammonia as a green fuel and hydrogen carrier for vehicular applications," *Journal of Power Sources*, vol. 185, no. 1, pp. 459–465, 2009. https://doi.org/10.4236/aces.2023.133018

[7] R. Lan, J. T. S. Irvine, and S. Tao, "Ammonia and related chemicals as potential hydrogen carriers for marine energy systems," *Applied Energy*, vol. 327, 2023. https://doi.org/10.4236/sgre.2025.169010

[8] M. Reiter and S.-C. Kong, "Combustion and emissions characteristics of compression-ignition engine using dual ammonia–diesel fuel," *Fuel*, vol. 90, no. 1, pp. 87–97, 2011. https://doi.org/10.1016/j.fuel.2010.07.055

[9] K. Ryu, G. Zacharakis-Jutz, and S.-C. Kong, "Performance and emissions of compression-ignition engine using ammonia–diesel dual fuel," *Applied Energy*, vol. 113, pp. 488–499, 2014. https://doi.org/10.1016/j.apenergy.2013.07.065

[10] Arkadiusz Jamrozik, Wojciech Tutak, Michał Pyrc, Karol Grab-Rogaliński, "Experimental study on ammonia-diesel co-combustion in a dual-fuel compression ignition engine" JournaloftheEnergyInstitute115(2024)101711. https://doi.org/10.1016/j.joei.2024.101711

[11] Leilei Xu [a], Shijie Xu [a], Xue-Song Bai a, Juho Aleksi Repo [b], Saana Hautala [b], Jari Hyvönen.,"Performance and emission characteristics of an ammonia/diesel dual-fuel marine engine" Renewable and Sustainable Energy Reviews 185 (2023) 113631. https://doi.org/10.1016/j.rser.2023.113631

[12] Ebrahim Nadimi, Grzegorz Przybyła, Michał T. Lewandowski, Wojciech Adamczyk., "Effects of ammonia on combustion, emissions, and performance of the ammonia/diesel dual-fuel compression ignition engine"., Journal of the Energy Institute 107 (2023) 101158. https://doi.org/10.1016/j.joei.2022.101158

[13] Lay, H. T., Tang, N., Arangaswamy, V., Ibrahim, I., & Liu, M. (2025). Role of neat biodiesel as pilot fuel in dual-fuel combustion for maritime decarbonization. *Biofuels*, 1–16. https://doi.org/10.1080/17597269.2025.2567726

[14] M. Lapuerta, O. Armas, and J. Rodríguez-Fernández, "Effect of biodiesel fuels on diesel engine emissions," *Progress in Energy and Combustion Science*, vol. 34, no. 2, pp. 198–223, 2008. https://doi.org/10.1016/j.pecs.2007.07.001

[15] S. K. Hoekman, A. Broch, C. Robbins, E. Ceniceros, and M. Natarajan, "Review of biodiesel composition, properties, and specifications," *Renewable and Sustainable Energy Reviews*, vol. 16, pp. 143–169, 2012. doi:10.1016/j.rser.2011.07.143

[16] Paramvir Singh, S.R. Chauhan, Varun Goel, "Assessment of diesel engine combustion, performance and emission characteristics fuelled with dual fuel blends" Renewable Energy, Vol. 125, September 2018, 501-510. https://doi.org/10.1016/j.renene.2018.02.105

[17] Kyong-Hyon KimandKyeong-Ju Kong, " 1D–3DCoupling for Gas Flow Analysis of the Air-Intake System in a Compression Ignition Engine". Mar. Sci. Eng. 2021, 9, 553. https://doi.org/10.3390/jmse9050553

[18] A. L. Yakovenkoa, M. G. Shatrova, L. N. Golubkova, E. A. Savastenkoa, and Yu. V. Trofimenkoa, " 3D Modeling in the Design and Researches of Internal Combustion Engines". Russian Engineering Research, 2022, Vol. 42, No. 11, pp. 1178–1181. DOI: 10.3103/S1068798X22110247

[19] ANSYS Inc., *ANSYS Forte Theory Guide*. Canonsburg, PA, USA: ANSYS, 2023.

[20] Tianwei Yang, Yu Yin, Hua Zhou, Zhuyin Ren," Review of Lagrangian stochastic models for turbulent combustion". Acta Mechanica Sinica (2021) 37(10):1467–1488 https://doi.org/10.1007/s10409-021-01142-7

[21] Liu, Jinlong, "Investigation of Combustion Characteristics of a Heavy-Duty Diesel Engine Retrofitted to Natural Gas Spark Ignition Operation" (2018). Graduate Theses, Dissertations, and Problem Reports. 3713. https://researchrepository.wvu.edu/etd/3713

[22] Stefano Frigo, Roberto Gentili, "Analysis of the behaviour of a 4-stroke Si engine fuelled with ammonia and hydrogen". International Journal of Hydrogen Energy. Vol. 38, Issue 3, 2013, 1607-161. http://dx.doi.org/10.1016/j.ijhydene.2012.10.114

[23] Heywood, J.B. *Internal Combustion Engine Fundamentals, 2nd Ed.*, McGraw-Hill, 2018.

[24] J. A. Miller and C T. Bowman, "Mechanism and Modeling of Nitrogen Chemistry in Combustion, Prog. Energy Combust. Sci. 1989, Vol. 15. pp. 287-338 Pnnted in Great Britain. All rights reserved.

[25] Turns, S.R. *An Introduction to Combustion*, McGraw-Hill. 2000

[26] R. Stone, "Introduction to Internal Combustion Engines," 3rd Edition, McMillan Press, London, 1999.

[27] [W. Tutak and A. Jamrozik, "Analysis of the Application of Ammonia as a Fuel for a Compression-Ignition Engine," Jun. 01, 2025, Multidisciplinary Digital Publishing Institute (MDPI). doi: 10.3390/en18123217.

[28] M. Lang, Y. Su, Y. Wang, Y. Zhang, B. Wang, and S. Chen, "Experimental study on the effects of pilot injection strategy on combustion and emission characteristics of ammonia/diesel dual fuel engine under low load," Energy, vol. 303, Sep. 2024, doi: 10.1016/j.energy.2024.131913.

[29] R. Chen et al., "Engine-out emissions from an ammonia/diesel dual-fuel engine – The characteristics of nitro-compounds and GHG emissions," Fuel, vol. 362, Apr. 2024, doi: 10.1016/j.fuel.2023.130740.

[30] L. Xu, S. Xu, X. S. Bai, J. A. Repo, S. Hautala, and J. Hyvönen, "Performance and emission characteristics of an ammonia/diesel dual-fuel marine engine," Renewable and Sustainable Energy Reviews, vol. 185, Oct. 2023, doi: 10.1016/j.rser.2023.113631.

[31] Y. Ma, J. Gao, Z. Wang, P. Zhang, X. Liu, and H. Yu, "Combustion and emission characteristics of ammonia-diesel marine high pressure direct injection low-speed dual-fuel engine," Sci. Rep., vol. 15, no. 1, Dec. 2025, doi: 10.1038/s41598- 025-049

[32] Y. Ma, J. Gao, Z. Wang, P. Zhang, X. Liu, and H. Yu, "Combustion and emission characteristics of ammonia-diesel marine high pressure direct injection low-speed dual-fuel engine," Sci. Rep., vol. 15, no. 1, Dec. 2025, doi: 10.1038/s41598- 025-0499